Lightweight Embedded Framework for Real-Time Fault Classification and Location in Radial Distribution Networks Under Distributed Generation

M. Lemkharbech, S. Sarih, Z. Boulghasoul, A. El Bacha, S. Chabaa

Abstract — **This study develops a low-complexity data-driven method for real-time fault classification, and localization on a 20 kV radial feeder, while accounting for the computational and memory constraints of embedded hardware. The proposed approach is motivated by the changes introduced by distributed generation (DG), which alters fault-current behavior and reduces the reliability of conventional impedance-based protection. These limitations are mainly caused by reverse power flows and the additional infeed contribution from DG units during fault conditions. The proposed hybrid architecture processes time- and frequency-domain features, including symmetrical components and wavelet energy, through a dual-stage inference chain. The first stage uses a Random Forest classifier for fault-type identification, while the second stage uses a Multi-Layer Perceptron (MLP) distance estimator for fault localization. Evaluation on 23,778 MATLAB/Simulink fault scenarios, was performed using a grouped scenario-level holdout split to reduce overlap between training and test cases. The proposed approach reduces the localization error compared with the conventional impedance method, which produced errors exceeding 14 km under DG operation. The Random Forest classifier achieved 99.44% fault-type accuracy, and the MLP estimator reached a Mean Absolute Error (MAE) of 93.8 m, with localization accuracy of 99.51% within 1 km. Analytical resource profiling estimates less than 300 KB Flash and under 50 µs execution time, assuming a Cortex-M4F/M7-class target, pending hardware-in-the-loop validation.**

I. INTRODUCTION

The increasing penetration of Distributed Generation (DG), especially photovoltaic generation, has changed the operating conditions of radial distribution networks. These networks were historically planned and protected under the assumption of unidirectional power flow from the main substation to downstream loads [1], [2]. With DG connected along the feeder, this assumption is no longer valid in all operating states. During a fault, the current measured at the feeder head may depend on the upstream source, the DG contribution, the fault resistance, the inception angle, and the fault position. This behavior complicates both protection coordination and fault location.

In DG-penetrated feeders, fault currents may decrease, increase, or reverse direction depending on the network condition. As a result, conventional overcurrent-based protection may lose selectivity and dependability [3], [4]. Fault localization is affected as well. An inaccurate distance estimate increases the search area for maintenance crews and delays isolation and restoration. In this context, rapid fault localization becomes operationally critical. Fast identification of faulted segments allows utilities to expedite isolation and restoration, directly improving continuity of service metrics, specifically the System Average Interruption Duration Index (SAIDI) and the System Average Interruption Frequency Index (SAIFI), and minimizing Energy Not Supplied (ENS).

Fault-location methods are commonly classified into impedance-based, traveling-wave, and data-driven approaches [5], [6]. Impedance-based methods remain attractive because they are simple and rely on voltage and current measurements that are usually available at the substation. Their accuracy, however, deteriorates in active feeders, where the apparent impedance seen from the source side is affected by fault resistance and DG infeed [7]. Traveling-wave methods can provide sub-kilometer accuracy, but they require high-frequency sampling, wideband sensing, and accurate timing. These requirements limit their use in conventional medium-voltage distribution feeders, especially when large-scale deployment is considered [8].

Machine-learning methods have recently received increasing attention for fault detection, classification, and localization. Models such as Random Forests, neural networks, SVM, and k-NN can learn fault signatures from simulated or recorded cases and have reported promising diagnostic performance [9], [10]. Yet, many studies still emphasize accuracy while giving less attention to the conditions under which the method would be deployed. In practice, a feeder-head diagnosis function must operate with a limited number of measurements, a compact feature set, bounded inference time, and a memory footprint compatible with IEDs, RTU gateways, or microcontroller-class devices [11]. This gap between

M. Lemkharbech is with the System Engineering and Applications Laboratory, Cadi Ayyad University, Marrakesh, Morocco (phone: 002126-2512-5376, e-mail: m.lemkharbech.ced@uca.ac.ma).

S. Sarih is with the Systems Engineering and Decision Support Laboratory, ENSA, Ibn Zohr University, Agadir 80000, Morocco (e-mail: saad.sarih@edu.uiz.ac.ma).

Z. Boulghasoul is with the System Engineering and Applications Laboratory, Cadi Ayyad University, Marrakesh, Morocco (e-mail: z.boulghasoul@uca.ma).

A. El Bacha is with the System Engineering and Applications Laboratory, Cadi Ayyad University, Marrakesh, Morocco (e-mail: a.elbacha@uca.ac.ma).

S. Chabaa is with the Systems Engineering and Decision Support Laboratory, ENSA, Ibn Zohr University, Agadir 80000, Morocco (e-mail: s.chabaa@uiz.ac.ma).

predictive performance and deployment feasibility remains a key issue for practical fault diagnosis in active distribution networks.

To address this issue, this paper proposes a lightweight data-driven framework for real-time fault diagnosis and localization in a 20 kV radial feeder with photovoltaic DG. The proposed architecture follows a two-stage structure. The first stage performs fault-type classification using a Random Forest classifier. The second stage estimates the fault location using a Multi-Layer Perceptron (MLP) regressor. This separation is intentional: fault-type identification is a discrete classification task, while fault localization requires distance-sensitive information and a different learning behavior.

The proposed framework is evaluated on 23,778 MATLAB/Simulink fault scenarios covering different fault types, fault locations, fault resistances, inception angles, and DG operating states. To avoid overly optimistic results caused by random mixing of similar simulated cases, the evaluation uses a grouped scenario-level holdout split. Scenarios sharing the same DG state, fault type, fault resistance, and inception angle are assigned either to the training set or to the test set, but not to both. The RF–MLP pipeline is compared with SVM-RBF, k-NN, and a conventional impedance-based method. In addition to classification and localization metrics, the study reports analytical estimates of Flash memory, RAM usage, and inference time under a compact Cortex-M-class implementation assumption.

The contribution lies in the design of a deployment-oriented diagnosis chain that combines protection-oriented feature engineering, a two-stage RF–MLP structure, DG-aware scenario generation, grouped evaluation, and embedded resource profiling. The results show that accurate fault classification and sub-kilometer localization can be achieved in the studied active feeder while keeping the inference chain within the estimated resource envelope of low-cost embedded targets. Hardware-in-the-loop validation and field-data assessment remain necessary steps before practical deployment.

II. Proposed Framework and Theoretical Modeling

A. Global Architecture of the Proposed Framework

The proposed framework uses three-phase voltage and current measurements recorded at the substation. The signals are processed over a fixed window. A feature extraction block calculates a compact input vector. The same normalized feature vector is then used by two models: a Random Forest classifier for fault-type identification and an MLP regressor for fault-distance estimation. The global architecture of the proposed framework is detailed in figure 1.

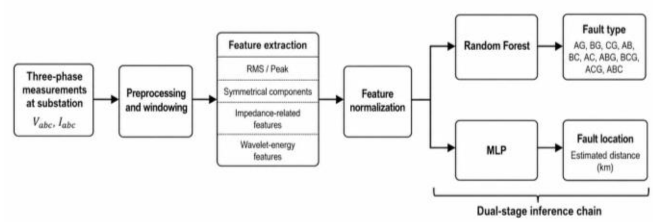

Figure 1. Global architecture of the proposed RF–MLP fault diagnosis framework.

B. Features Extraction

The feature vector is designed to be physically interpretable and suitable for embedded implementation. It contains the following groups of features:

- RMS and Peak of V_{abc} and I_{abc}: used to capture magnitude variations and phase asymmetry during the fault.
- Sequence components V012 and I012: used to describe unbalance and ground involvement; they are standard protection theory and cheap to compute.
- Ground discrimination ratio I0/I1(Ratio_I0I1): critical to separate ABC (ideally I0=0) from ABCG (nonzero I0).
- Impedance magnitude Zmag and imaginary component Ximag: support distance sensitivity while enabling partial physical compensation under DG infeed.
- Wavelet energy (log scale) on currents (Db4 level 1 energy): captures transient content associated with fault inception, with moderate overhead compared to raw-signal deep models.

The selection balances interpretability (sequence features) and discriminative power under non-stationary conditions (wavelet energy), while keeping a footprint suitable for embedded targets.

C. Random Forest Classifier

The Random Forest classifier is used for fault-type identification. It maps the feature vector (x) to one of the ten fault classes (Eq.1):

$$\hat{y} = \text{mode}\left\{h_1(x), h_2(x), ..., h_T(x)\right\} \quad (1)$$

where h_t is the prediction of tree (t), and (T) is the number of trees.

The Random Forest is selected for the classification stage because it can handle nonlinear separation between classes and interactions between features. This is relevant for distinguishing LL and LLG faults when the ground current is reduced by high fault resistance or modified by DG contribution.

D. MLP Fault-Location Model

The MLP is used for fault-distance estimation. The target output is the fault distance d in kilometers. The input is the normalized feature vector $x \in R^p$. The output is the estimated distance $\hat{d}$.

A feed-forward MLP with two hidden layers is used (figure 2). The forward propagation is:

$$z^{(1)} = W^{(1)}x + b^{(1)}, \; a^{(1)} = f(z^{(1)}),$$
$$z^{(2)} = W^{(2)} a^{(1)} + b^{(2)}, \; a^{(2)} = f(z^{(2)}),$$
$$\hat{d} = W^{(3)}a^{(2)} + b^{(3)}.$$

The output layer is linear because the target is a continuous distance. The model is trained by minimizing the Mean Squared Error (Eq.2):

$$L_{MSE} = \frac{1}{N}\sum_{i=1}^{N}(d_i - \hat{d}_i)^2 \qquad (2)$$

Input features are normalized using the training-set statistics. The same normalization parameters are then applied to validation and test data. This avoids leakage of test-set information into the learning process.

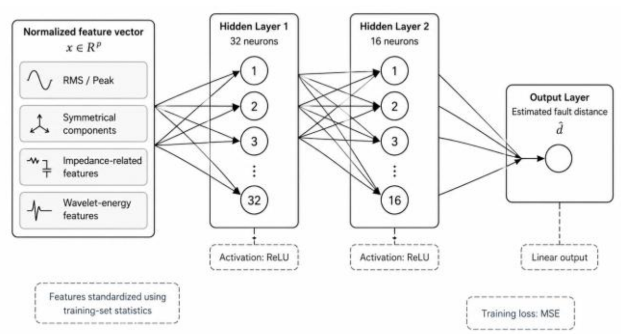

Figure 2. MLP architecture used for fault-distance estimation.

E. Training and Evaluation Procedure

The training and evaluation process is summarized below.

- Define the 20 kV radial feeder, DG connection, load, cable parameters, and fault block in MATLAB/Simulink.
- Generate fault scenarios by varying fault type, location, fault resistance, inception angle, and DG operating state.
- Record (V_{abc} and I_{abc}) at the substation.
- Extract RMS, peak, symmetrical component, impedance-related, and wavelet-energy features.
- Normalize the feature matrix using training-set statistics.
- Split the dataset using a grouped scenario-level holdout strategy. Each group is defined by DG operating state, fault type, fault resistance, and inception angle. All samples belonging to the same scenario group are assigned either to the training set or to the test set, but not to both.
- Train the Random Forest classifier using fault-type labels.
- Train the MLP regressor using fault-distance labels.
- Evaluate classification using Accuracy, Precision, Recall, and F1-score [13].
- Evaluate localization using MAE, RMSE, and Accuracy (<1 km) [14].
- Estimate Flash memory, RAM use, and inference time from model size and operation counts.

III. System Model and Methodology

A. Distribution Network Model

The case studied is a 20 kV radial distribution feeder modeled in MATLAB/Simulink, with the following characteristics:

TABLE I. PARAMETERS OF THE SIMULATED 20 KV DG-INTEGRATED DISTRIBUTION FEEDER

Parameter	***Value***
Grid nominal voltage	20 kV (MV)
Grid Frequency	50 Hz
Network structure	Radial feeder
Source model	Ideal three-phase voltage source
Short-circuit level	12 MVA
Feeder	Underground cable
Length	20 km
Positive-sequence parameters	R_1=0.22Ω/km, L_1=1.3 mH/km, C_1=9.0 µF/km
Zero-sequence parameters	R_0=0.66 Ω/km, L_0=3.9 mH/km, C_0=9.0 µF/km
Load apparent power	10 MVA
DG technology	Photovoltaic (PV) source
DG rated power	10 MVA
DG control	ON / OFF modes
Fault scenarios	AG, BG, CG, AB, BC, AC, ABG, BCG, ACG, ABC
Fault resistance	From 1 m Ω to 100 Ω

The single line diagram of studied radial feeder is detailed in figure 3.

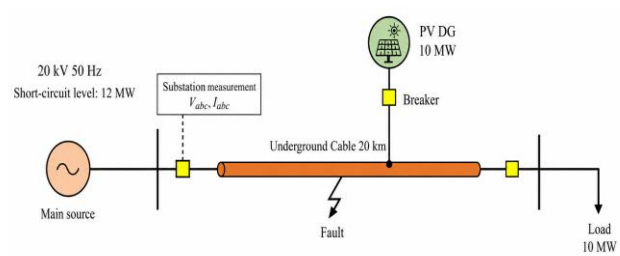

Figure 3. Single-line diagram of the studied 20 kV radial feeder

B. Fault scenario generation

The MATLAB/Simulink model (figure 4) includes the source, cable feeder, PV-DG branch, load, fault block, measurement blocks, and signal export blocks. Voltage and current waveforms are recorded at the substation side. These signals are then processed in MATLAB for feature extraction and model training.

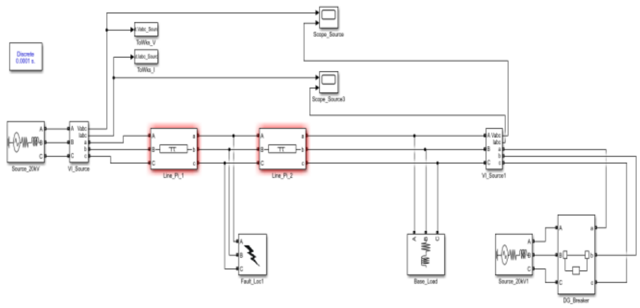

Figure 4. Block representation of the MATLAB/Simulink model

A dataset of 23,778 fault scenarios was generated using MATLAB/Simulink with the SimPowerSystems toolbox. The fault scenarios encompass the following parameter variations:

TABLE II. FAULT SCEANRIO GENERATION

Category	Parameters of Fault scenario		
	Parameter	***Value/range***	***Notes***
Dataset	Generation toolchain	MATLAB/Simulink	Time-domain EMT-style simulations
Fault classes	Total classes	10	Multi-class labeling
	SLG faults	AG, BG, CG	Single line-to-ground
	LL faults	AB, BC, AC	Line-to-line
	LLG faults	ABG, BCG, ACG	Double line-to-ground
	LLL/LLLG	ABC/ABCG	All lines
Fault location	Distance	0–20 km	Along the feeder (step: 2Km)
Fault resistance (R_f)	Range	[0.001 0.01 0.1 1 10 50 100] Ω	Bolted to high impedance
Fault inception angle	Range	0°–330°:30°	Captures impact of fault initiation at different points on voltage waveform
DG operating state	Mode 0	DG OFF	Unidirectional power flow
	Mode 1	DG ON	Bidirectional flow with DG contribution
Acquisition	Signals recorded	V_{abc} , I_{abc}	Measurement at substation: Three-phase waveforms

Each fault scenario is simulated for a duration sufficient to capture post-fault behavior, typically 5–10 cycles. Voltage and current waveforms are recorded at a sampling rate of 10 kHz. ABC and ABCG faults are merged into one symmetrical-fault class because their protection response is similar and their electrical signatures are close in the considered measurement configuration [12].

IV. Experimental Results

The framework was evaluated on an unseen test set. This section presents a quantitative benchmark of the algorithms, analyzing their accuracy, regression precision, and hardware efficiency.

A. Fault Classification Results

The classification module identifies the fault type among 10 classes. Table III summarizes the results obtained on the test set.

TABLE III. COMPARATIVE FAULT CLASSIFICATION METRICS

Model	Metrics			
	Accuracy	***Precision***	***Recall***	***F1-Score***
Random Forest	0.994	0.995	0.995	0.995
MLP	0.922	0.931	0.925	0.928
k-NN	0.903	0.902	0.899	0.900
SVM-RBF	0.876	0.895	0.875	0.884

Table III shows that the Random Forest provides the best classification performance, reaching 99.44% accuracy. The confusion matrix in Figure 5 confirms a dominant diagonal structure, with limited errors mainly between electrically close LL and LLG faults under high-resistance conditions.

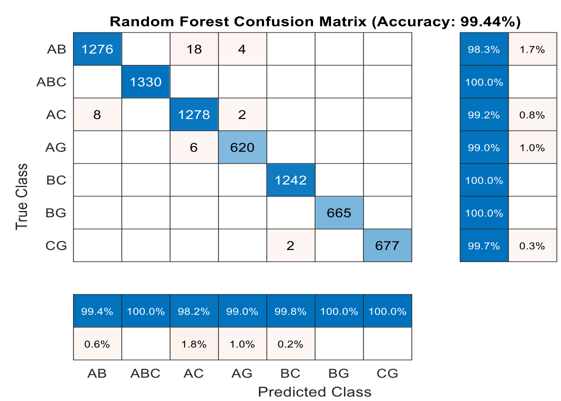

Figure 5. The confusion matrix for the Random Forest

B. Fault Localization Results

After classification, the fault distance is estimated. Table IV compares the proposed AI-based estimators against the conventional Impedance Method.

Due to the complexity of implementing a full TW chain (MHz sampling and wideband sensing), TW results are adopted from the literature as a reference benchmark (MAE=0.150 km, RMSE=0.200 km, Accuracy (<1 km)=99.00%) and are reported as approximately invariant under DG-ON conditions [15], [16].

TABLE IV. COMPARATIVE FAULT LOCALIZATION METRICS

Method	Metrics				
	Global	***RMSE***	***Accuracy***	***MAE***	***MAE***

	MAE (km)	*(km)*	*(<1km)*	*(DG-OFF) (km)*	*(DG-ON) (km)*
TW (literature)	0.150	0.200	99.00%	0.150	0.150
Impedance Method (Baseline)	14.177	20.859	9.44%	3.348	24.262
MLP	0.094	0.249	99.51%	0.052	0.132
RF	0.221	0.469	95.90%	0.105	0.330
SVM-RBF	0.959	1.626	75.35%	0.595	1.298
k-NN	0.092	0.462	97.84%	0.024	0.156

Table IV summarizes the fault-location performance of conventional and data-driven methods under operating variability and DG integration. The impedance method gives the largest error. Its global MAE is 14.177 km, and its MAE under DG-ON reaches 24.262 km. This confirms the sensitivity of apparent-impedance location to DG infeed. The MLP gives the best overall localization result when MAE, RMSE, and Accuracy (<1 km) are considered together. Its global MAE is 0.094 km and 99.51% of its estimates are within 1 km of the actual fault position. k-NN gives a similar global MAE, but its RMSE is higher, which indicates more large-error cases.

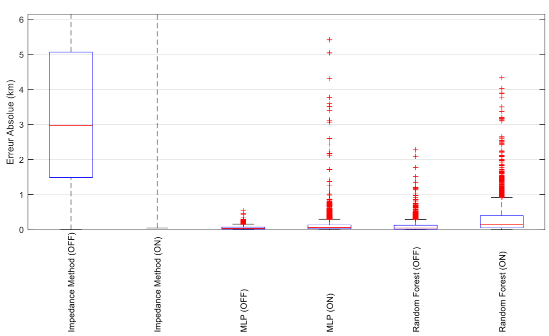

Figure 6. Boxplot analysis of localization errors under DG-OFF and DG-ON conditions.

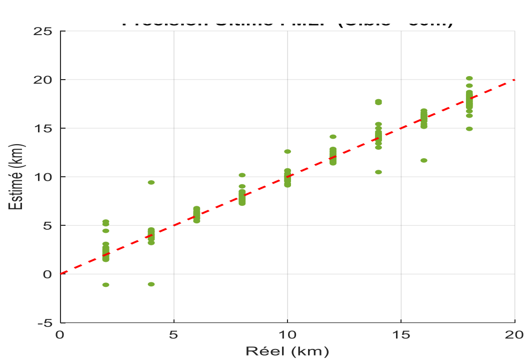

Figure 7. Scatter Plot of Predicted vs. Actual Fault Distances using the MLP model.

- Robustness Analysis: The stability of the solution under varying grid topologies is presented in Figure 6. While the median error of the MLP increases slightly from 52 m (DG-OFF) to 132 m (DG-ON), the error distribution remains compact. This demonstrates that the neural network implicitly learns to compensate for the infeed factor, maintaining sub 200m precision without requiring remote measurements.
- Regression Reliability: The scatter plot in Figure 7 confirms the linearity of the prediction across the entire feeder length (0–20 km), validating that the model performs consistently regardless of the fault. Figure 7 visualizes the reliability of the models. The MLP ensures that 99.51% of fault estimations fall within 1 km of the true location, a critical requirement for maintenance crew dispatch.

The conventional Impedance Method shows severe degradation with a Mean Absolute Error (MAE) exceeding 14 km (Table IV). This confirms that analytical methods cannot compensate for the infeed current without external communication. In contrast, the proposed D-MLP model achieves a Global MAE of 93.8 meters (0.094 km), reducing the error by a factor of 150.

C. Embedded Feasibility and Resource Estimation

Practical deployment requires low memory use and bounded latency. Table V gives the estimated resource requirements for the tested models. These figures are comparative estimates derived from model parameterization and operation counts. They assume a compact float32 implementation on a microcontroller-class target, such as ARM Cortex-M4F or Cortex-M7 with hardware floating-point support.

TABLE V. EMBEDDED RESOURCE ESTIMATES

Model	**Resources**			
	Flash (Code & Params)	***RAM (Buffers)***	***Inference Time***	***Complexity***
MLP	~12 KB	<2 KB	~8 µs	Low (~3.5 kFLOPs)
Random Forest	~250 KB	~15 KB	~35 µs	Medium (branching)
k-NN	~50 KB	~5 KB	~60 µs	High (distance search)
SVM-RBF	>500 KB	>32 KB	>2000 µs	Very High (kernel evaluations)

The MLP locator has the most predictable inference time because it uses fixed-count matrix-vector operations. The Random Forest classifier is also fast, but its Flash use depends on the number of trees and nodes. k-NN and SVM-RBF are less attractive for strict embedded constraints because their inference cost depends on stored prototypes or support vectors.

The complete RF–MLP inference pipeline is estimated to require less than 300 KB Flash and execute under 50 µs. These figures do not include acquisition overhead, full feature-extraction time, or real-time operating-system scheduling. They should therefore be read as feasibility indicators, not as hardware measurements.

V. Discussion

A. Interpretation of Classification Results

The classification results show a clear advantage for the Random Forest model. This behavior is not incidental. The selected feature space combines quantities with different physical meanings: sequence components, impedance-related indicators, wavelet-energy features, and DG operating information. Under fault-resistance variation, inception-angle changes, and DG contribution, the separation between classes is no longer governed by simple linear boundaries. RF is well suited to this situation because its ensemble structure partitions the feature space locally and captures interactions between variables without imposing a single global decision surface. The most delicate distinction remains the separation between LL and LLG faults. This is expected. When the fault resistance increases, the ground-current component may become weak, and the zero-sequence signature loses part of its discriminative strength. The remaining off-diagonal terms in the confusion matrices are therefore not random errors; they correspond to operating cases where grounded and ungrounded multi-phase faults produce partially overlapping signatures.

B. Interpretation of Localization Results

For fault localization, the MLP provides the most balanced performance. The relation between the extracted features and the fault position is nonlinear, especially when DG infeed modifies the voltage-current relationship seen from the substation. A shallow MLP can approximate this mapping while keeping the model size limited, which is important for embedded implementation. Its output remains stable across the tested operating conditions, with a low average error and a limited dispersion of large deviations. The comparison with k-NN is particularly informative. Although k-NN reaches a global MAE close to that of the MLP, its RMSE is higher. This indicates the presence of occasional large errors. In operational fault-location support, such outliers matter. A single large distance error may direct field crews toward the wrong feeder section and delay restoration. For this reason, the MLP is retained as the preferred locator, not only because of its average accuracy, but also because of its more controlled error distribution.

C. Effect of DG Connection

The DG operating state has a visible impact on all localization methods. The effect is most severe for the impedance-based baseline. Its MAE increases from 3.348 km under DG-OFF operation to 24.262 km under DG-ON operation. This sharp degradation confirms that the apparent impedance measured at the substation is strongly affected by the additional infeed current and no longer reflects only the line section between the source and the fault.

The MLP is also affected by DG connection, but to a much lesser extent. Its MAE increases from 0.052 km to 0.132 km. The increase is measurable, yet it remains limited compared with the impedance baseline. This suggests that the selected features, together with the nonlinear mapping learned by the MLP, capture part of the DG-induced change in the voltage-current relationship. This conclusion must, however, be interpreted within the simulated operating domain. Field measurements and hardware-in-the-loop tests are still required before extending the claim to real feeders.

D. Robustness and Generalization

The generated dataset covers several sources of variability: fault type, fault location, fault resistance, inception angle, and DG operating state. These variations provide a useful controlled environment for comparing the models. They do not, however, reproduce the full complexity of field operation. In practice, measured signals may be affected by noise, current-transformer saturation, voltage-transformer errors, missing channels, topology changes, load fluctuations, and uncertainty in line parameters. Each of these factors can alter the extracted features and, consequently, the model decision. Further robustness assessment is therefore necessary. Future tests should include controlled noise injections, missing-channel conditions, CT saturation modeling, feeder reconfiguration, and changes in DG location or penetration level. These experiments would provide a clearer view of the transferability of the proposed framework beyond the simulated cases used in this study.

E. Limits of the Present Validation

The main limitation of this work is the exclusive reliance on MATLAB/Simulink simulations. The simulated dataset allows a repeatable and systematic evaluation over many fault conditions, but it cannot replace field evidence. COMTRADE records, disturbance files, incident logs, and laboratory measurements are needed to assess how the method behaves with real sensors, real switching events, and imperfect network data. A second limitation concerns embedded validation. The reported Flash memory, RAM usage, and inference-time values are analytical estimates derived from model size and operation counts. No physical microcontroller, IED, or hardware-in-the-loop platform was used in the present version. A real implementation may introduce additional constraints related to acquisition timing, feature-extraction overhead, task scheduling, numerical precision, and memory allocation. The third limitation is linked to feeder specificity. The case studied is a 20 kV radial feeder with defined cable parameters, load level, and PV-DG configuration. Applying the same framework to other feeders would require additional testing, and retraining or calibration, depending on the topology, grounding arrangement, DG location, and load profile.

These limitations set the scope of the present contribution. The proposed framework should therefore be understood as a simulation-validated and deployment-oriented diagnosis method, not as a field-certified protection function. Its practical value will depend on the next validation steps: field records, HIL testing, and implementation on an actual embedded target.

VI. Conclusion

This study proposed a lightweight RF–MLP framework for fault diagnosis in DG-integrated radial feeders. The RF classifier achieved 99.44% fault-type accuracy, while the MLP locator reached an MAE of 0.094 km, with 99.51% of estimates within 1 km. Unlike impedance-based methods, the proposed approach remained stable under DG-ON operation. These results confirm that accurate diagnosis and embedded feasibility can be addressed together through a compact, deployment-oriented inference chain.

The main contribution of the work lies in this deployment-oriented formulation. The framework uses standard voltage and current measurements available at the substation, without relying on wideband sensing, MHz-range acquisition, or synchronized remote measurements. This is important for practical integration into existing IED, RTU, or feeder-head automation environments. The embedded assessment also supports this direction: under a compact float32 implementation assumption on a Cortex-M-class architecture, the complete RF–MLP inference chain is estimated to require less than 300 KB of Flash memory and to execute in less than 50 µs. These figures, however, remain analytical estimates. They indicate feasibility, not hardware validation. A physical implementation would still need to account for acquisition time, feature-extraction overhead, scheduling constraints, numerical precision, and memory allocation on the selected target.

Several points must be addressed before the framework can be considered ready for field deployment. The present validation relies on MATLAB/Simulink simulations, which provide controlled and repeatable operating conditions but do not reproduce all disturbances encountered in real feeders. Future work should therefore include multi-source validation using COMTRADE records, field disturbance files, laboratory measurements, time-synchronized recordings, and incident logs. Robustness must also be quantified under measurement noise, missing voltage or current channels, current-transformer saturation, voltage-transformer errors, line-parameter uncertainty, feeder reconfiguration, and changes in DG location or penetration level. In parallel, hardware-in-the-loop testing and implementation on an actual microcontroller or IED-class platform are necessary to confirm the reported resource estimates. Additional developments, such as probabilistic confidence bounds, feature-attribution analysis, quantization, pruning, and fixed-point deployment, would further improve both operator trust and industrial readiness.

References

[1] L. Souto, J. Meléndez and S. Herraiz, "Fault Location in Low Voltage Smart Grids Based on Similarity Criteria in the Principal Component Subspace," 2020 IEEE Power & Energy Society Innovative Smart Grid Technologies Conference (ISGT), Washington, DC, USA, 2020, pp. 1-5, doi: 10.1109/ISGT45199.2020.9087707.

[2] Z. Zhang, W. Jiang, J. Geng, X. Deng and X. Li, "Fault Diagnosis Based on Non-Negative Sparse Constrained Deep Neural Networks and Dempster–Shafer Theory," in IEEE Access, vol. 8, pp. 18182-18195, 2020, doi: 10.1109/ACCESS.2020.2966260.

[3] Y. Zhao, M. Zhou, X. Xu, N. Zhang and H. Zhang, "Fault Diagnosis Based on Space Mapping and Deformable Convolution Networks," in IEEE Access, vol. 8, pp. 212599-212607, 2020, doi: 10.1109/ACCESS.2020.3040448.

[4] R. Marino, C. Wisultschew, A. Otero, J. M. Lanza-Gutierrez, J. Portilla and E. d. l. Torre, "A Machine-Learning-Based Distributed System for Fault Diagnosis With Scalable Detection Quality in Industrial IoT," in IEEE Internet of Things Journal, vol. 8, no. 6, pp. 4339-4352, March15, 2021, doi: 10.1109/JIOT.2020.3026211.

[5] M. Zhao and M. Barati, "A Real-Time Fault Localization in Power Distribution Grid for Wildfire Detection Through Deep Convolutional Neural Networks," in IEEE Transactions on Industry Applications, vol. 57, no. 4, pp. 4316-4326, July-Aug. 2021, doi: 10.1109/TIA.2021.3083645.

[6] O. T. Ibitoye, M. O. Onibonoje and J. O. Dada, "Machine Learning Based Techniques for Fault Detection in Power Distribution Grid: A Review," 2022 3rd International Conference on Electrical Engineering and Informatics (ICon EEI), Pekanbaru, Indonesia, 2022, pp. 104-107, doi: 10.1109/IConEEI55709.2022.9972279.

[7] A. Ghaderi, H. L. Ginn, et H. A. Mohammadpour, « High impedance fault detection: A review », Electric Power Systems Research, vol. 143, p. 376 388, févr. 2017, doi: 10.1016/j.epsr.2016.10.021.

[8] X. Zhang, Y. Hu, J. Deng, H. Xu and H. Wen, "Feature Engineering and Artificial Intelligence-Supported Approaches Used for Electric Powertrain Fault Diagnosis: A Review," in IEEE Access, vol. 10, pp. 29069-29088, 2022, doi: 10.1109/ACCESS.2022.3157820.

[9] Q. Li et al., "Incipient Fault Detection in Power Distribution System: A Time–Frequency Embedded Deep-Learning-Based Approach," in IEEE Transactions on Instrumentation and Measurement, vol. 72, pp. 1-14, 2023, Art no. 2507914, doi: 10.1109/TIM.2023.3250220.

[10] Q. -H. Ngo, B. L. H. Nguyen, J. Zhang, K. Schoder and T. Vu, "Graphical Learning Based Fault Detection and Classification in Distribution Systems," 2024 IEEE International Conference on Communications, Control, and Computing Technologies for Smart Grids (SmartGridComm), Oslo, Norway, 2024, pp. 588-593, doi: 10.1109/SmartGridComm60555.2024.10738028.

[11] M. M. Zaben, M. Y. Worku, M. A. Hassan and M. A. Abido, "Machine Learning Methods for Fault Diagnosis in AC Microgrids: A Systematic Review," in *IEEE Access*, vol. 12, pp. 20260-20298, 2024, doi: 10.1109/ACCESS.2024.3360330.

[12] P. J. Lagace, L. A. Dessaint, M. Lavoie, J. Mahseredjian and A. Chartrand, "Transient short circuit current calculation using decoupled networks," in *IEEE Transactions on Power Delivery*, vol. 14, no. 3, pp. 1110-1114, July 1999, doi: 10.1109/61.772381.

[13] S. Sarih, S. Chabaa, Z. Boulghasoul, A. Tajer, et E. B. Abdelhadi, " Wavelet-based fault detection and classification in MV grids using neural models: case study of Moroccan distribution system ", International Journal of Emerging Electric Power Systems, déc. 2025, doi: 10.1515/ijeeps-2025-0187.

[14] J. Wang *et al*., "Smart Fault Detection, Classification, and Localization in Distribution Networks: AI-Driven Approaches and Emerging Technologies," in *IEEE Access*, vol. 13, pp. 141664-141693, 2025, doi: 10.1109/ACCESS.2025.3596791.

[15] O. Naidu and A. K. Pradhan, "A Traveling Wave-Based Fault Location Method Using Unsynchronized Current Measurements," in IEEE Transactions on Power Delivery, vol. 34, no. 2, pp. 505-513, April 2019, doi: 10.1109/TPWRD.2018.2875598.

[16] Y. Xu, S. Zhang, Y. Liu, Y. Nie and L. Yi, "Fault Location on Distribution Cables Using Traveling Waves: a Field Data Study," 2023 IEEE Power & Energy Society General Meeting (PESGM), Orlando, FL, USA, 2023, pp. 1-5, doi: 10.1109/PESGM52003.2023.10252745.